Proceedings of the 4th
International Conference on Robotics and Mechatronics
October 26-28, 2016, Tehran, Iran

An Observer-Based Adaptive Impedance-Control for Robotic Arms: Case Study in SMOS Robot

Soheil Gholami, Arash Arjmandi, and Hamid D. Taghirad, *Senior Member, IEEE*.
Advanced Robotics and Automated Systems (ARAS), Industrial Control Center of Excellence (ICCE),
Faculty of Electrical Engineering, K.N. Toosi University of Technology, Tehran, Iran.
Email: sgholami@ee.kntu.ac.ir, arash.arj@gmail.com, taghirad@kntu.ac.ir.

***Abstract*—In this paper an adaptive output-feedback impedance control is proposed to be used in environment-machine interaction applications. The proposed control is designed to achieve a desired robot impedance in the presence of possible dynamical parameter uncertainties. A high-gain observer is utilized in the control structure to achieve this objective by using only position feedback of robot joints, which in turn, reduces implementation costs and eliminates additional sensor requirements. Stability of the overall system is analyzed through input to state stability analysis. Finally, to evaluate the presented structure, computer simulations are provided and the scheme effectiveness is verified.**

***Keywords*—Adaptive control, impedance control, high-gain observer, input to state stability, eye-surgery.**

I. Introduction

Besides the mechanical design, control systems play a fundamental role in achieving a desired performance in different robotic tasks. Depending on the task, different control objectives can be considered. For example in painting task, the robot's end-effector moves freely in the workspace, while in other tasks such as robotic surgery, end-effector's motion can be constrained by interactions with the environment. Generally one may find two scenarios for most of the tasks, free and constrained motions. Trajectory tracking, or position control is the prime objective in free motion control, while in the latter, both position and force controls are important.

Various control methods have been proposed to deal with the problem of interaction control. The notion of *impedance control*, which was first introduced by Hogan [1] is of great interest among other proposed methods due to its ability for the applicability of simultaneous position and force control. Admittance control is also widely used as another method for interaction control, which is the inverse of impedance control and controls the ratio of motion output to force input. In [2] both schemes have been compared by making use of a non-adaptive control strategy.

Dynamics modeling of robotic arms introduces various uncertainties in its parameters. Therefore, robust and adaptive control schemes are more proper alternatives to tackle this problem. In some robust control schemes such as sliding mode control, the structure and bounds of the uncertainty is assumed to be known. As an example of the sliding mode control design, one may refer to [3] in which impedance control has been used as well. In adaptive schemes uncertainty bounds are not needed to be known a priori, which makes this schemes to be used widely, and in these schemes adaptation rule can well handle the parametric uncertainty effects. Several researches have been focused on the realization of adaptive controllers, however most of them use joints positions and velocities as feedback signals, including [4]. Using velocity sensors makes the feedback signal noisy, thus the resultant performance may be deteriorated for high-gain controllers. Furthermore, velocity sensors increase the robot weight and implementation costs. Consequently, it is much preferable to use the output-feedback instead of the state-feedback routines. As mentioned in [5], this may be accomplished by using observers to estimate velocity signals. In addition, it should be noted that in impedance control, which is realized in some of the adaptive structures by making use of output-feedback routines such as [6], direct force measurements are also needed. However, force sensors are expensive and may also introduce design limitations. Hence, it is relevant to estimate external force signals besides the velocity estimations, as well.

To handle the direct measurement challenges, sliding mode observers [7], high-gain observers [5], and dirty filters [8] are reported in the literature. In [7], it is proved that the observation errors converge exponentially to zero by making use of the sliding mode observer. However, this method is based on the assumption that the initial joint position estimation error must be zero. On the other hand, this limitation does not exist in the high-gain observers, and furthermore, the high-gain property make the observer to behave like a linear systems. Moreover, in dirty filters the force estimation is not realized, and therefore, this is not a preferable choice in the impedance control strategies. One may see [8] as an example of adaptive output-feedback structure, followed by a simple non-adaptive control scheme that presented in [9]. In these references two adaptive controllers have been introduced without considering impedance in which one of them uses a dirty filter to estimate the velocity signal. However, the force signal, which is needed in an impedance control strategy, is not estimated. Furthermore, in [5], joint velocity estimation is also realized by using a high-gain observer. However, the stability of the observer-based adaptive control is analyzed by some assumptions that make the control law relatively conservative.

978-1-5090-3222-8/16/$31.00 ©2016 IEEE

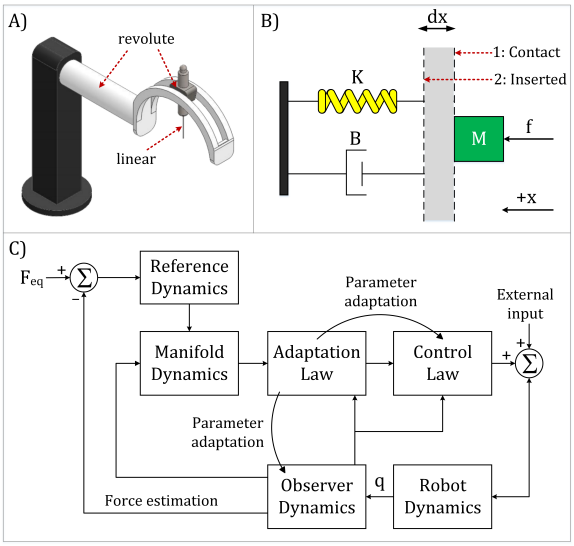

Fig. 1: A) SMOS, B) MSD system, C) the proposed control scheme

Additionally, the proposed method is not based on impedance and joint space control is the prime objective.

Moreover, most of the proposed adaptive impedance control schemes are designed without considering the fact that one of the important aspects of the impedance notion find its application in the teleoperation systems, where the communication delay causes challenges in the overall closed loop stability of the system. For an example in [6] different adaptive impedance controllers are realized, and their closed loop stability are studied by means of Lyapunov second method and Barbalat's lemma. Robustness with respect to time delay and external inputs has not been addressed. Moreover, that work uses the state-feedback control law and a force sensor. Impedance control in the teleoperation systems has been studied in several works, including [10], where an input to output stability based impedance controller is utilized by using feedback linearization scheme.

Inspired by [8] and [5], in this work an adaptive control scheme has been proposed, which by using an adaptive high-gain observer, the velocity and force estimations are made possible. Considering the variable time delay in the teleoperation applications, the stability of the control structure, which is utilized in the robot task space, is provided in the sense of ISS property. Furthermore, computer simulation results are presented to show the effectiveness of the proposed algorithm. In order to show the proposed controller effectiveness, SMOS (Stereotaxical Micro-telemanipulator for Ocular Surgery) eye-surgery robot [11] is considered as a case study, which its computer-aided design (CAD) is shown in Fig. 1(A) and its dynamical equations are given in Appendix.1.

II. Proposed Control Scheme

As illustrated in Fig. 1(B), force $f(t)$ which is exerted to an object (contact) and the corresponding displacement $dx(t)$ (insertion) may be used to define the impedance of a mechanical system. In frequency domain, the linear time invariant (LTI) impedance is defined, by making use of the Laplace transformation, as $Z(s) := \frac{F(s)}{dX(s)}$. One of the typical impedance definitions is a mass-spring-damper (MSD), also called Kelvin-Voigt, system which is defined as follows.

$$Z(s) := M\,s^2 + B\,s + K, \tag{1}$$

where the constant and positive-definite matrices M, B, and K represent the desired inertia, damping, and stiffness of the object, respectively. Although (1) is defined for one degree of freedom (DoF) motion, the generalization to several DoFs may be considered as well. In addition, this concept may be extended to torque and angular motions [12].

Robot dynamical behavior may be generally described as follows [13]:

$$H(q)\ddot{q} + C(q,\,\dot{q})\dot{q} + G(q) = u_c + u_{ext}, \tag{2}$$

where u_{ext} is the external torques that robot may experience, while the other parameters are defined in [13]. In this paper, the main idea of the proposed controller is to use a reference impedance model, based on (1), as:

$$M\left[\ddot{x}_{ref} - \ddot{x}_{eq}\right] + B\left[\dot{x}_{ref} - \dot{x}_{eq}\right] + K\left[x_{ref} - x_{eq}\right] = f_{ext}, \tag{3}$$

where, x_{eq} is the desired trajectory, x_{ref} denotes the reference position, and f_{ext} is the external force vector. To achieve the desired dynamical behavior, a manifold may also be defined, on which robot positions in task space asymptotically converge to the reference model position $x \to x_{ref}$. Such manifold may be considered as [4]:

$$s := \dot{q} - \dot{q}_{dr}, \tag{4}$$

where, $\dot{q}_{dr}$ is the first time derivative of an auxiliary reference trajectory, q_{dr}. In what follows $\dot{q}_{dr}$ and its derivative are presented, where the eigenvalues of matrix Λ are considered to be on the open left half plane.

$$\dot{q}_{dr} = J^{-1}(q)\left[\dot{x}_{ref} + \Lambda\left\{x_{ref} - x\right\}\right], \tag{5}$$

$$\ddot{q}_{dr} = J^{-1}(q)\left[\ddot{x}_{ref} + \Lambda\left\{\dot{x}_{ref} - \dot{x}\right\} - \dot{J}(q)\,\dot{q}_{dr}\right]. \tag{6}$$

Once all the system trajectories approach s, we have:

$$s = 0 \Rightarrow \dot{x}_{ref} - \dot{x} + \Lambda\left[x_{ref} - x\right] = 0. \tag{7}$$

Thus, if the control strategy forces the trajectories of system to $s = 0$, we will obtain the main control objective after a time constant, i.e. $x \to x_{ref}$.

Consider the following control law:

$$\begin{aligned} u &= \hat{H}(q)\,\ddot{\hat{q}}_{dr} + \hat{C}(q,\,\dot{\hat{q}})\,\dot{q}_{dr} + \hat{G}(q) - \Psi\,\hat{s} \\ &= A(q,\,\dot{\hat{q}},\,\dot{q}_{dr},\,\ddot{\hat{q}}_{dr})\,\hat{p} - \Psi\,\hat{s}, \end{aligned} \tag{8}$$

where, $\hat{H}(q)$, $\hat{C}(q,\,\dot{\hat{q}})$, and $\hat{G}(q)$ are estimation of the dynamic matrices, $\Psi \in \mathrm{R}^{\dim(u)\times\dim(q)}$ is a Hurwitz control gain matrix, $\hat{s}$ is the manifold estimation, whose estimation error is defined by $\tilde{s} := \hat{s} - s$, $A(\cdot) \in \mathrm{R}^{\dim(u)\times\dim(p)}$ is the dynamic

regressor matrix, and $\hat{p} \in \mathrm{R}^{\dim(p)}$ is the dynamical parameter estimation, updated by the following adaptation law [8]

$$\dot{\hat{p}} = -\Omega\, A^T(q,\, \dot{\hat{q}},\, \dot{q}_{dr},\, \ddot{\hat{q}}_{dr})\, \hat{s} - \kappa\, [\tilde{p} + \bar{\tilde{p}}]\,, \tag{9}$$

in which, $\Omega \in \mathrm{R}^{\dim(p)\times\dim(p)}$ is a Hurwitz adaptation gain matrix, κ is a positive constant, $\tilde{p} := \hat{p} - p$ is the parameter adaptation error, and $\bar{\tilde{p}}$ represents the nominal value of the parameters. Furthermore, variables $\dot{\hat{q}}$, , $\ddot{\hat{q}}_{dr}$ and $\hat{s}$ are updated by a high gain estimator, defined by [14]:

$$\begin{aligned} \dot{\hat{x}}_1 &= \hat{x}_2 + \frac{\phi_1}{\varepsilon}\, \tilde{y}, \\ \dot{\hat{x}}_2 &= H^{-1}(\hat{x}_1)\, [u - \Delta_R - C(\hat{x}_1,\, \hat{x}_2)\, \hat{x}_2 - G(\hat{x}_1)] + \frac{\phi_2}{\varepsilon^2}\, \tilde{y}, \end{aligned} \tag{10}$$

where $\hat{x}_1 := \hat{q}$, $\hat{x}_2 := \dot{\hat{q}}$, $\tilde{y} := y - \hat{y}$, and $\phi_1,\, \phi_2,\, \varepsilon > 0$ are chosen according to the above mentioned considerations. In (10) dynamic uncertainty, Δ_R, may be estimated as:

$$\Delta_R(\hat{x}_1,\, \hat{x}_2,\, t) = H(\hat{x}_1)\, \frac{\phi_2}{\varepsilon^2}\, \tilde{y}. \tag{11}$$

The overall control scheme is illustrated in Fig. 1(C).

Theorem 1: System described by (2), (3), (8), (9), and (10), with state $X = [s,\, \tilde{p},\, \tilde{\eta}]$ and inputs $U = [\hat{u}_h,\, p^\star]$ is ISS with proper control gains.

Proof 1: Consider the following ISS-Lyapunov (ISS-L) candidate function

$$V\,(s,\, e,\, \tilde{p},\, \tilde{n}) = \frac{1}{2}\left(s^T H\, s + \mu\, e^T e + \tilde{p}^T \Omega^{-1} \tilde{p} + \tilde{\eta}^T P_o\, \tilde{\eta}\right) \tag{12}$$

in which, μ is a positive constant and P_o is a positive-definite matrix. In what follows it is proven that (12) is indeed an ISS-L function. Based on matrix eigen-value inequality [8], one may obtain two positive constants V_1 and V_2 such that the following inequality holds on a compact set, like D.

$$V_1 \le V\,(s,\ e,\ \tilde{p},\ \tilde{n}) \le V_2, \tag{13}$$

Next, differentiate $V(t)$ with respect to time:

$$\dot{V}\,(t) = s^T H \dot{s} + 0.5\, s^T \dot{H}\, s + \mu\, e^T \dot{e} + \tilde{p}^T \Omega^{-1} \dot{\tilde{p}} + \tilde{\eta}^T P_o\, \dot{\tilde{\eta}}. \tag{14}$$

To obtain an upper bound for $\dot{V}(t)$, few terms have been considered and each of them is studied, one by one, as follows. Base on (4):

$$\dot{s} = H^{-1}(q)\, [u_c + u_{ext} - C(q,\, \dot{q})\, \dot{q} - G(q)] - \ddot{q}_{dr}. \tag{15}$$

Substitute (8) in (15), and derive the first term of $\dot{V}$ as:

$$\begin{aligned} s^T H(q)\, \dot{s} = s^T &\left[\hat{H}(q)\ \ddot{\hat{q}}_{dr} + \hat{C}(q,\, \dot{\hat{q}})\, \dot{q}_{dr} + \hat{G}(q) - \Psi\, \hat{s}\right] \\ &- s^T\, [H(q)\ \ddot{q}_{dr} + C(q,\, \dot{q})\, \dot{q} + G(q)] + s^T u_{ext}, \end{aligned}$$

where $C(q,\, \dot{q})\dot{q}$ may be replaced by $C(q,\, \dot{q})s + C(q,\, \dot{q})\dot{q}_{dr}$ and $\hat{s} := \tilde{s} + s$. Thus, in regressor representation, we have:

$$\begin{aligned} s^T\, H(q)\, \dot{s} + 0.5\, s^T\, \dot{H}(q)\, s = &-s^T\, \Psi\, s - s^T\, \Psi\, \tilde{s} + s^T u_{ext} \\ &+ s^T \left[A(\hat{\Theta})\, \hat{p} - A(\Theta)\, p\right], \end{aligned} \tag{16}$$

in which, the skew-symmetric property of $\dot{H} - 2\,C$ [13], is used to eliminate $0.5\, s^T \dot{H}(q)\, s$. In addition, to simplify notations two new variables $\Theta := [q,\, \dot{q},\, \dot{q}_{dr},\, \ddot{q}_{dr}]$ and $\hat{\Theta} := \left[q,\, \dot{\hat{q}},\, \dot{q}_{dr},\, \ddot{\hat{q}}_{dr}\right]$ are defined. With the aid of linear Algebra, one may show that the following equality holds:

$$A(\hat{\Theta})\, \hat{p} - A(\Theta)\, p = A(\hat{\Theta})\, \tilde{p} + A(\hat{\Theta})\, p - A(\Theta)\, p. \tag{17}$$

Substitute (17) in (16), and conclude that:

$$\begin{aligned} s^T H(q)\, \dot{s} + 0.5\, s^T \dot{H}(q)\, s = &-s^T\, \Psi\, s - s^T\, \Psi\, \tilde{s} + \tilde{p}^T A^T(\hat{\Theta}) s \\ &+ s^T u_{ext} + s^T \left[A(\hat{\Theta})\, p - A(\Theta)\, p\right]. \end{aligned} \tag{18}$$

In addition, manifold (4) results into $\dot{e} = J(q)\, s - \Lambda\, e$; therefore, $\mu\, e^T\, \dot{e}$ is derived as follows:

$$\mu\, e^T \dot{e} = -\mu\, e^T\, \Lambda\, e + \mu\, e^T\, J(q)\, s. \tag{19}$$

Dynamic parameters are considered to be constant with respect to time, i.e. $\dot{\tilde{p}} = \dot{\hat{p}}$. Thus, by utilizing (9) we have:

$$\tilde{p}^T\ \Omega^{-1}\, \dot{\tilde{p}} = -\tilde{p}^T\ A^T(\hat{\Theta})\, \hat{s} - \kappa\, \tilde{p}^T\, \Omega^{-1} \tilde{p} - \kappa\, \tilde{p}^T\, \Omega^{-1} p^\star.$$

Hence,

$$\begin{aligned} \dot{V} = &-s^T \Psi\, s - \mu\, e^T \Lambda\, e - \kappa\, \tilde{p}^T \Omega^{-1} \tilde{p} + s^T u_{ext} \\ &- s^T \Psi \tilde{s} - \kappa\, \tilde{p}^T\, \Omega^{-1} p^\star - \tilde{p}^T A^T(\hat{\Theta}) \tilde{s} + \mu e^T J(q) s \\ &+ s^T \left[A(\hat{\Theta})\, p - A(\Theta)\, p\right] + \tilde{\eta}^T P_o \dot{\tilde{\eta}}, \end{aligned} \tag{20}$$

in which by using matrix inequality property [8], for the first three terms, the following inequalities hold.

$$\begin{aligned} &-s^T \Psi\, s \le -\lambda_{\min}\{\Psi\}\, s^T s, \ \ -\mu\, e^T \Lambda\, e \le -\mu\, \lambda_{\min}\{\Lambda\}\, e^T e, \\ &-\kappa\, \tilde{p}^T \Omega^{-1} \tilde{p} \le -\kappa\, \lambda_{\min}\left\{\Omega^{-1}\right\} \tilde{p}^T \tilde{p}. \end{aligned} \tag{21}$$

Moreover, function $\Xi(\Theta) := A(\Theta)\, p$ is Lipschitz, i.e. there exists a positive constant like l such that:

$$\Xi^\star = \left\|\Xi(\hat{\Theta}) - \Xi(\Theta)\right\| \le l \left\|\hat{\Theta} - \Theta\right\|. \tag{22}$$

Furthermore, Young inequality implies the following inequalities.

$$\begin{aligned} s^T\, u_{ext} &\le \frac{c_1}{2}\, s^T\, s + \frac{1}{2\, c_1}\, {u_{ext}}^T\, u_{ext}, \\ \kappa\, \tilde{p}^T \left[-\Omega^{-1} p^\star\right] &\le \frac{\kappa\, c_2}{2}\, \tilde{p}^T\, \tilde{p} + \frac{\kappa}{2\, c_2}\, {p^\star}^T\, {\Omega^{-1}}^T \Omega^{-1}\, p^\star, \\ \mu\, e^T\, J(q)\, s &\le \frac{\mu\, c_3}{2}\, e^T\, e + \frac{\mu}{2\, c_3}\, s^T\, J(q)^T\, J(q)\, s, \\ s^T\, \Psi\, \tilde{s} &\le \frac{c_4}{2}\, s^T\, s + \frac{1}{2\, c_4}\, \tilde{s}^T\, \Psi^T\, \Psi\, \tilde{s}, \\ \tilde{p}^T\, A^T(\hat{\Theta})\, \tilde{s} &\le \frac{c_5}{2}\, \tilde{p}^T\, \tilde{p} + \frac{1}{2\, c_5}\, \tilde{s}^T\, A(\hat{\Theta})\, A^T(\hat{\Theta})\, \tilde{s}, \\ s^T\, \Xi^\star &\le \frac{c_6}{2}\, s^T\, s + \frac{1}{2\, c_6}\, \Xi^{\star T} \Xi^\star, \end{aligned} \tag{23}$$

Hence, by using (21)-(23) in (20), an upper bound for $\dot{V}(t)$ is obtained as follows:

$$\begin{aligned} \dot{V}(t) \le &-a_1\, s^T s - a_2\, \tilde{p}^T\, \tilde{p} - a_3\, e^T\, e + a_4\, {u_{ext}}^T u_{ext} \\ &+ a_5\, {p^\star}^T p^\star + a_6\, \tilde{s}^T \tilde{s} + a_7\, \tilde{\Theta}^T \tilde{\Theta} + \tilde{\eta}^T P_o \dot{\tilde{\eta}}, \end{aligned} \tag{24}$$

where,

$$\begin{aligned} a_1 :=& \lambda_{\min}\{\Psi\} - \left\{\frac{c_1 + c_4 + c_6}{2} + \frac{\mu}{2\, c_3} \lambda_{\max}\left\{J^T J\right\}\right\} \\ a_2 :=& \kappa\, \lambda_{\min}\left\{\Omega^{-1}\right\} - \frac{\kappa\, c_2 + c_5}{2} \\ a_3 :=& \mu\left[\lambda_{\min}\{\Lambda\} - \frac{c_3}{2}\right], \quad a_4 := \frac{1}{2\, c_1}, \quad a_7 := \frac{l^2}{2\, c_6} \\ a_5 :=& \frac{\kappa}{2\, c_2} \lambda_{\max}\left\{{\Omega^{-1}}^T \Omega^{-1}\right\}, \\ a_6 :=& \frac{1}{2\, c_4} \lambda_{\max}\left\{\Psi^T \Psi\right\} + \frac{1}{2\, c_5} \lambda_{\max}\left\{A(\hat{\Theta})\, A^T(\hat{\Theta})\right\}. \end{aligned} \tag{25}$$

From (4), following equality may be concluded.

$$\tilde{s} = \hat{s} - s \Rightarrow \dot{\tilde{s}} = \ddot{\tilde{q}} \Rightarrow \tilde{s} = [0 \quad I]\, \tilde{\eta}, \tag{26}$$

which yields to:

$$\tilde{s}^T \tilde{s} = \|\tilde{s}\|^2 \leq \|S^\star\|^2 \, \|\tilde{\eta}\|^2 . \tag{27}$$

Moreover, a similar results may be obtained as $\tilde{\Theta} := \hat{\Theta} - \Theta = \Theta^\star \, \tilde{\eta},$, where the non-zero elements of 4×2 block matrix $\Theta^\star$ are $\tilde{\theta}_{22} = I_{n\times n}$ and $\tilde{\theta}_{42} = J^{-1}(q)\,\Lambda\, J(q)$. Therefore, the following ineqality is also satisfied.

$$\tilde{\Theta}^T \tilde{\Theta} = \left\| \tilde{\Theta} \right\|^2 \leq \|\Theta^\star\|^2 \|\tilde{\eta}\|^2. \tag{28}$$

Now substitute (27) and (28) in (24), and simplify the time derivative of $V(\cdot)$ as:

$$\begin{aligned} \dot{V}(t) \leq & -a_1 \, s^T s - a_2 \, \tilde{p}^T \, \tilde{p} - a_3 \, e^T \, e \\ & + a_4 \, {u_{ext}}^T \, u_{ext} + a_5 \, {p^\star}^T \, p^\star - a_6^\star \, \tilde{\eta}^T \, \tilde{\eta} \end{aligned} \tag{29}$$

in which $a_6^\star$ is defined as follows:

$$a_6^\star := \lambda_{\min} \left\{ \varepsilon^{-1} W_o \right\} - 2\,\delta_o^\star \, \|P_o\| - a_6 \, \|S^\star\|^2 - a_7 \, \|\Theta^\star\|^2.$$

in which, the stability analysis, provided in [14], is used for high gain observer term, i.e. $\tilde{\eta}^T P_o \dot{\tilde{\eta}}$. Based on the ISS theorem provided in [15], inequalities (13) and (29) indicate that $V(\cdot)$ is a ISS-L function, which concludes the theorem.

The other part of closed loop system is the reference system (3), which is represented in state space as follows.

$$\dot{x} : = A_I \, x + B_I \left[\hat{f}_{ext} + f_{eq} \right], \tag{30}$$

where $f_{eq} := M\ddot{x}_{eq} + B\dot{x}_{eq} + Kx_{eq}$, $x = [x_{ref}^T, \, \dot{x}_{ref}^T]^T$, and

$$A_I := \begin{bmatrix} 0_{n\times n} & I_{n\times n} \\ -M_m^{-1} K_m & -M_m^{-1} B_m \end{bmatrix}, \quad B_I := \begin{bmatrix} 0 \\ M_m^{-1} \end{bmatrix}. \tag{31}$$

It may be shown that matrix A_I in (31) is Hurwitz, therefore, for any positive-definite matrix Q_I there exists a unique positive-definite matrix P_I such that the Lyapunov equation $A_I^T \, P_I + P_I \, A_I = -Q_I$ is satisfied. Hence, by choosing a Lyapunov function $V_{ref}(x) = 0.5\, x^T P_I \, x$ which is lower and upper bounded as well, the resultant time derivative of that function is derived as follows.

$$\dot{V}_{ref}(t) = -x^T \left[Q_I + A_I^T \, P_I \right] x + x^T \, P_I \, B_I \left[\hat{f}_{ext} + f_{eq} \right], \tag{32}$$

where by utilizing matrix [8] and Young inequalities we have:

$$\begin{aligned} \dot{V}_{ref}(t) \leq & - \left[\lambda_{\min} \left\{ Q_I + A_I^T \, P_I \right\} - \frac{\lambda_1}{2} \right] \|x\|^2 \\ & + \frac{1}{2\,\lambda_1} \|P_I\|^2 \|B_I\|^2 \|\hat{f}_{ext} + f_{eq}\|^2, \end{aligned} \tag{33}$$

which indicates that the reference model system is also ISS. Thus, the overall closed loop system is ISS by using the small gain theorem, i.e. $\gamma \times \gamma_{ref} < 1$, by choosing appropriate control parameters.

III. Simulation Results

In this section, computer simulations are presented by using the SMOS robot as a case study. SMOS has two rotational and one linear joints, and due to its spherical-like structure, by using the spherical coordinate, task and joint spaces are equivalent. This consideration is also reasonable in practice, because in Cartesian space robot is singular in its remote center of motion point (RCM). One may check the singularity of robot in RCM by substituting $q_3 = r_3$ in the following forward kinematic equation of SMOS.

$$x = (r_3 - q_3)\, s_2, \;\; y = (r_3 - q_3)\, c_2 \, c_1, \;\; z = -\,(r_3 - q_3)\, c_2 \, s_1.$$

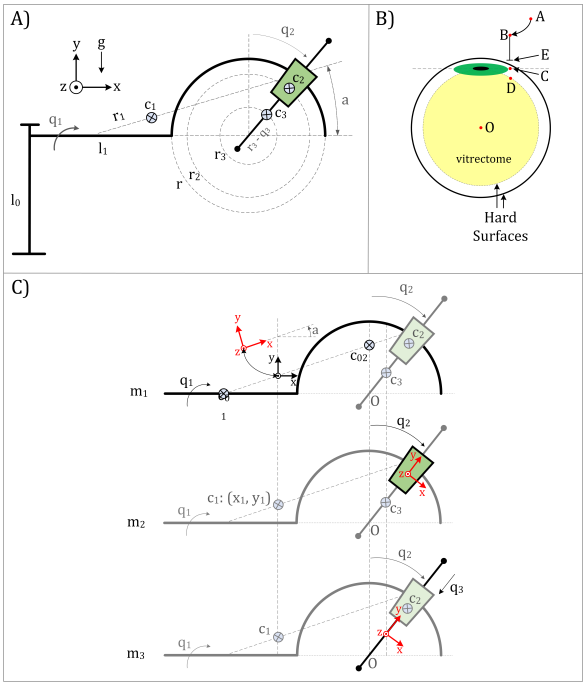

Fig. 2: A) SMOS structure, B) end-effector insertion to the human eye, C) SMOS dynamics chain

where $s_1 := \sin(q_1)$, $s_2 := \sin(q_2)$, $c_1 := \cos(q_1)$, and $c_2 := \cos(q_2)$. Hence, in spherical coordination the joint and task space arrays are the same, i.e. $q = x$, which yields the Jacobian matrix is an identity matrix. Furthermore, as the proposed scheme is model-based, the dynamical matrices are needed. In Appendix.1, the dynamical matrices are derived, using Euler-Lagrange formulation.

Impedance plays a significant role in the constraint motions. SMOS finds its application in eye-surgeries, in which robot end-effector should be inserted to the interior region of the eye through RCM point. Based on this fact, it is considered that robot's end-effector is interacting with a human eye. As it is shown in Fig. 2(B), suppose motion starts somewhere outside the eye like point A, according to the following desired trajectory.

$$\begin{aligned} & x_{eq,3}(t) = a_1 + a_2\, t + a_3\, t^2 + a_4\, t^3, \; t \leq 10(sec) \\ & x_{eq,3}(t) = 0, \qquad\qquad\quad 10(sec) < t \leq 20(sec) \end{aligned} \tag{34}$$

In addition, $x_{eq,1}(t) = x_{eq,2}(t) = 0$. The above equations represent the insertion task. It should be noted that for simplicity only the insertion DoF has been considered. Moreover, in simulation time $t_f = 20\,(\text{sec})$, the coefficients are $a_1 = x_{3,\,i}$, $a_2 = \dot{x}_{3,\,i}$, and

$$\begin{aligned} a_3 &= +3\, {t_f}^{-2} \left[x_{3,\,f} - x_{3,\,i} \right] - {t_f}^{-1} \left[\dot{x}_{3,\,f} + \dot{x}_{3,\,i} \right], \\ a_4 &= -2\, {t_f}^{-3} \left[x_{3,\,f} - x_{3,\,i} \right] + {t_f}^{-2} \left[\dot{x}_{3,\,f} + \dot{x}_{3,\,i} \right], \end{aligned} \tag{35}$$

where $x_{3,\,i} = -0.005\,(\text{m})$ and $x_{3,\,f} = 0.005\,(\text{m})$. The initial and final values of $\dot{x}_3$ are considered to be zero, i.e. $\dot{x}_{3,\,i} = \dot{x}_{3,\,f} = 0$. As the operation starts, robot experiences both free (point A to C) and constraint (point C to D)

motions. At point B, the first two joints of robot are reached to their desired fixed positions, $x_1 = x_2 = 0$; however, the third joint changes according to (34). Robot end-effector first experiences the contact at point C, where a stiff layer impedes the motion. To analyze the effect of layer characteristics, three different stiffness have been considered for the environment, $k_1 = 1(N/m)$, $k_2 = 100(N/m)$, and $k_3 = 1000(N/m)$ with a fixed damping $b = 1\,(\mathrm{N}\cdot\mathrm{sec}^2/\mathrm{m})$, which is described by the following Kelvin-Voigt relation:

$$f_{x_3} = k\,\delta x_3 + b\,\delta\dot{x}_3, \quad x_3 \geq x_{e,3}, \tag{36}$$

where, the insertion to the layer is defined by $\delta x_3 := x_3 - x_{e,3}$, with $x_{e,3} = 0\,(\mathrm{m})$.

Here, The desired mechanical impedance is tuned as follows. The desired inertia, damping, and stiffness matrices are set to $M = 100\,I_{3\times3}$, $B = 500\,I_{3\times3}$, and $K = 5000\,I_{3\times3}$, respectively, where I denotes the unity matrix. To reach the objectives, control parameters are set to $\Psi = 10\,I_{3\times3}$, $\Lambda = 100\,I_{3\times3}$, $\Omega^{-1} = 10^{-5}I_{9\times9}$, and $\kappa = 1$. Furthermore, the observer parameters are set to $\phi_1 = 5$, $\phi_2 = 6$, and $\varepsilon = 0.0025$.

As it may be seen in Fig. 3, last DoF best tracks the desired trajectory in the presence of lower layer stiffness. This is illustrated in the top part of this figure. Furthermore it may be noted that more stiff environment leads to trajectory tracking deterioration, starting from $t = 5(\mathrm{sec})$ due to the unconstraint motion, as shown in the lower part of the figure. In this figure solid and dashed lines represent the desired and robot trajectories, respectively. In addition, control efforts and the external efforts estimation that are caused by the interaction, are shown in Fig. 4, where the effect of different stiffness may be clearly seen from time $t = 5(\mathrm{sec})$. In this figure, control efforts and external force estimation are shown with solid and dashed lines, respectively.

Fig. 5 shows that the parameters converge to their real values with an appropriate accuracy after a time transient. It should be noted that all three simulations are performed with the same control and impedance parameters, and only layer stiffness are changed. These parameters may be tuned for higher stiffness to gain better trajectory tracking. To show the perfect trajectory tracking of the control scheme, it may be seen in Fig. 6, that with a rich desired trajectories (solid lines), made of several different sinusoidal terms, robot best follows the trajectories (dashed lines) with the same control parameters.

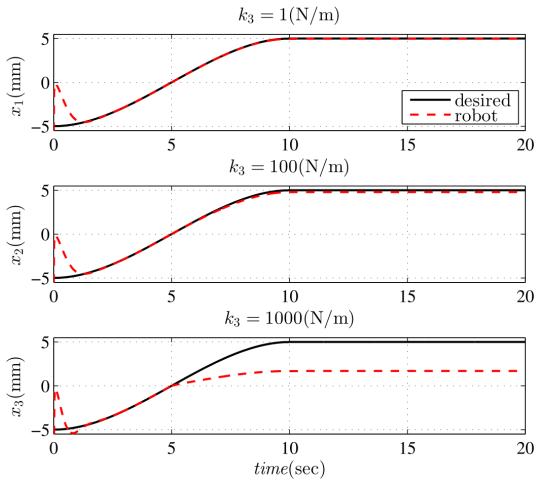

Fig. 3: Trajectory tracking

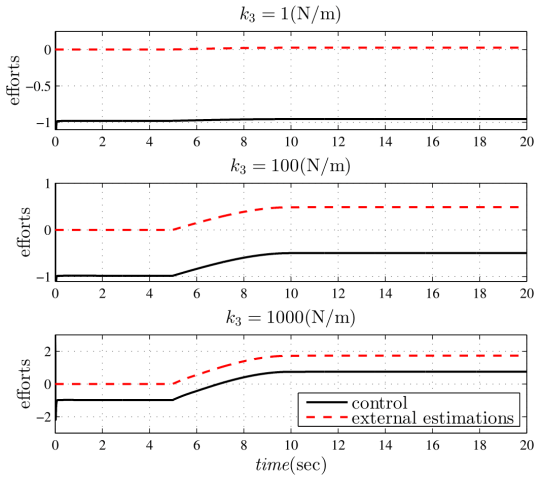

Fig. 4: Control efforts and the external effort estimations

IV. Concluding Remarks

In this article, an adaptive output-feedback impedance control scheme is developed for machine-environment interaction motions. Unlike the majority of existing impedance control schemes, in the proposed method, desired impedance is achieved by using only robots joint position feedbacks in the presence of various uncertainties in robots dynamics. This has been achieved using an adaptive high-gain observer that eliminates the requirements of expensive sensors for environment interaction forces and joint velocity measurements. It has been also proven that the closed-loop system, consisting adaptive impedance controller and high-gain observer, is input-to-state stable using an ISS Lyapunov candidate function. In order to validate the stability analysis and also demonstrate the performance of the proposed method numerical simulation results is given and analyzed.

V. Appendix 1

Using Figs. 2(A) and (C), SMOS dynamical equations may be derived by Lagrange method. Dynamical parameters p_i are:

$$\begin{aligned}
&p_1 = I_{x1} + I_{x2} + I_{x3} - [I_{x1} - I_{y1}]\,{s_a}^2 + m_1\,r_1^2\,s_a^2 + 2\,m_1\,r_1\,s_a\,y_1\\
&p_2 = m_2\,{r_2}^2 + m_3\,{r_3}^2, \quad p_3 = m_1\,{y_1}^2,\\
&p_4 = m_3, \quad p_5 = 2\,m_3\,r_3, \quad p_6 = I_{y2} + I_{y3} - I_{x2} - I_{x3},\\
&p_7 = I_{z2} + I_{z3}, \quad p_8 = m_2\,r_2, \quad p_9 = m_1\,y_1 + m_1\,r_1\,s_a,
\end{aligned}$$

The elements of inertia matrix $H_{3\times3}$ are:

$$\begin{aligned}
H_{11} &= p_1 + p_2 - p_2\,{s_2}^2 + p_3 + p_4\,{q_3}^2 - p_4\,{q_3}^2\,{s_2}^2\\
&\quad - p_5\,q_3 + p_5\,q_3\,{s_2}^2 + p_6\,{s_2}^2,\\
H_{22} &= p_2 + p_4\,{q_3}^2 - p_5\,q_3 + p_7, \quad H_{33} = p_4,\\
H_{21} &= H_{12} = 0, \quad H_{31} = H_{13} = 0, \quad H_{32} = H_{23} = 0,
\end{aligned} \tag{37}$$

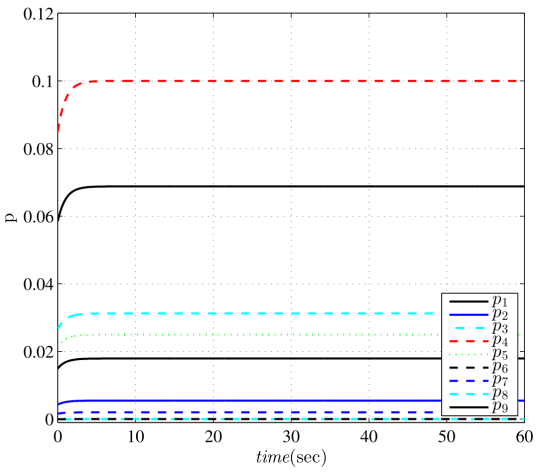

Fig. 5: Parameter adaptation

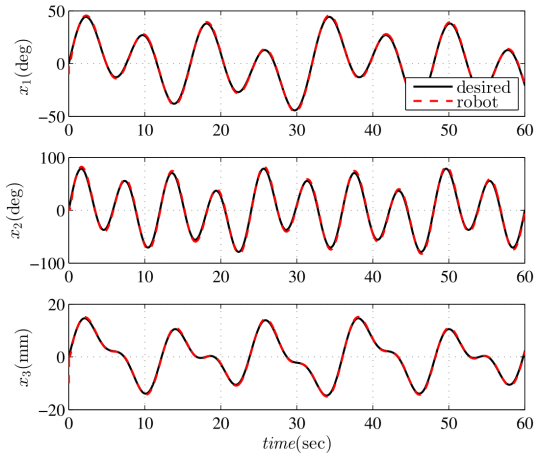

Fig. 6: Perfect trajectory tracking in free motion scenario

the elements of gravity $G_{3\times1}$ array are:

$$\begin{aligned} G_1 &= -g\, s_1\, [p_9 - p_4\, c_2\, q_3 + p_8\, c_2 + 0.5\, p_5\, c_2]\,, \\ G_2 &= -g\, c_1\, s_2\, [p_8 - p_4\, q_3 + 0.5\, p_5]\,, \quad G_3 = -g\, p_4\, c_1\, c_2, \end{aligned} \tag{38}$$

and elements of centrifuge and Coriolis matrix $C_{3\times3}$ are:

$$\begin{aligned} C_{11} &= -0.5\, \dot{q}_2\, ss_2\, \left[p_2 + p_4\, {q_3}^2 - p_5\, q_3 - p_6\right] \\ &\quad - 0.5\, \dot{q}_3\, [2\, p_4\, q_3 - p_5]\, \left[{s_2}^2 - 1\right], \\ C_{12} &= -0.5\, \dot{q}_1\, ss_2\, \left[p_2 + p_4\, {q_3}^2 - p_5\, q_3 - p_6\right], \\ C_{13} &= -0.5\, \dot{q}_1\, [2\, p_4\, q_3 - p_5]\, \left[{s_2}^2 - 1\right], \\ C_{21} &= 0.5\, \dot{q}_1\, ss_2\, \left[p_2 + p_4\, {q_3}^2 - p_5\, q_3 - p_6\right], \\ C_{22} &= p_4\, q_3\, \dot{q}_3 - 0.5\, p_5\, \dot{q}_3, \\ C_{23} &= p_4\, q_3\, \dot{q}_2 - 0.5\, p_5\, \dot{q}_2, \\ C_{31} &= 0.5\, \dot{q}_1\, [2\, p_4\, q_3 - p_5]\, \left[{s_2}^2 - 1\right], \\ C_{32} &= -p_4\, q_3\, \dot{q}_2 + 0.5\, p_5\, \dot{q}_2, \quad C_{33} = 0, \end{aligned} \tag{39}$$

where, $c_3 := \cos(q_3)$, $s_3 := \sin(q_3)$, $s_a = \sin(a)$, and $ss_2 := \sin(2q_2)$. To verify dynamical equations, a virtual SimMechanics model of SMOS robot has been utilized in a PD control loop, together with the derived dynamical equations. Control signal u_m is exerted to the virtual physical model of SMOS, which causes that model follows a rich desired trajectory. The resultant motions of the model enters the inverse version of the derived dynamics. As a result, the mathematical model input vector u_i is calculated. It should be noted that the proportional and derivative control gains are $k_p = 100$ and $k_d = 10$, respectively. Furthermore the rich trajectory is given by $x(t) = \sum_{i=1}^{6} a_i\, \sin(\omega_i\, t)$. Comparison between u_m and u_s proves the validity of the derived equations. The validation errors are in the order of 10^{-14}. Due to space limitation, the results are not displayed in here. However, a similar procedure is reported in [13]. Finally, the nominal values of the model parameters are given in Table I.

TABLE I: SMOS structural parameters

Parameter	Value	Quantity
$[I_{xx_1}, I_{yy_1}, I_{zz_1}]$	[0.01, 0.01, 0.01]	$\mathrm{Kg/m^2}$
$[I_{xx_2}, I_{yy_2}, I_{zz_2}]$	[0.001, 0.001, 0.001]	$\mathrm{Kg/m^2}$
$[I_{xx_3}, I_{yy_3}, I_{zz_3}]$	[0.001, 0.001, 0.001]	$\mathrm{Kg/m^2}$
$[r, r_1, r_2, r_3]$	[0.125, 0.086, 0.086, 0.086]	m
$[l_0, l_1, x_1, y_1]$	[0.41, 0.35, 0, 0]	m
$[m_1, m_2, m_3]$	[0.8, 0.25, 0.10]	Kg
a	90	deg

REFERENCES

[1] Neville Hogan. Impedance control: An approach to manipulation: Part iiimplementation. *Journal of dynamic systems, measurement, and control*, 107(1):8–16, 1985.

[2] Alin Albu-Schäffer and Gerd Hirzinger. Cartesian impedance control techniques for torque controlled light-weight robots. In *Robotics and Automation, 2002. Proceedings. ICRA'02. IEEE International Conference on*, volume 1, pages 657–663. IEEE, 2002.

[3] John M Daly and David WL Wang. Time-delayed output feedback bilateral teleoperation with force estimation for-dof nonlinear manipulators. *Control Systems Technology, IEEE Transactions on*, 22(1):299–306, 2014.

[4] Jean-Jacques E Slotine and Weiping Li. On the adaptive control of robot manipulators. *The international journal of robotics research*, 6(3):49–59, 1987.

[5] Kang Woong Lee and Hassan K Khalil. Adaptive output feedback control of robot manipulators using high-gain observer. *International Journal of Control*, 67(6):869–886, 1997.

[6] Mojtaba Sharifi, Saeed Behzadipour, and Gholamreza Vossoughi. Nonlinear model reference adaptive impedance control for human–robot interactions. *Control Engineering Practice*, 32:9–27, 2014.

[7] C Canudas De Wit and J-JE Slotine. Sliding observers for robot manipulators. *Automatica*, 27(5):859–864, 1991.

[8] Ilia G Polushin, Abdelhamid Tayebi, and Horacio J Marquez. Control schemes for stable teleoperation with communication delay based on ios small gain theorem. *Automatica*, 42(6):905–915, 2006.

[9] IG Polushin and HJ Marquez. Stabilization of bilaterally controlled teleoperators with communication delay: an iss approach. *International Journal of Control*, 76(8):858–870, 2003.

[10] Nam Duc Do and Toru Namerikawa. Impedance control for force-reflecting teleoperation with communication delays based on ios small gain theorem. In *ICCAS-SICE, 2009*, pages 4079–4086. IEEE, 2009.

[11] Aicha Guerrouad and Pierre Vidal. Smos: stereotaxical microtelemanipulator for ocular surgery. In *Engineering in Medicine and Biology Society, 1989. Images of the Twenty-First Century., Proceedings of the Annual International Conference of the IEEE Engineering in*, pages 879–880. IEEE, 1989.

[12] Hamid D Taghirad. *Parallel robots: mechanics and control*. CRC press, 2013.

[13] Ebrahim Abedloo, Soheil Gholami, and Hamid D Taghirad. Eye-rhas manipulator: From kinematics to trajectory control. In *Robotics and Mechatronics (ICROM), 2015 3rd RSI International Conference on*, pages 061–066. IEEE, 2015.

[14] Mohammad Motaharifar, Heidar A Talebi, Farzaneh Abdollahi, and Ahmad Afshar. Nonlinear adaptive output-feedback controller design for guidance of flexible needles. 2015.

[15] Eduardo D Sontag and Yuan Wang. On characterizations of the input-to-state stability property. *Systems & Control Letters*, 24(5):351–359, 1995.